

DRAFT

IDAHO NATIONAL LABORATORY PROGRAM TO OBTAIN BENCHMARK DATA ON THE
FLOW PHENOMENA IN A SCALED MODEL OF A PRISMATIC GAS-COOLED REACTOR
LOWER PLENUM FOR THE VALIDATION OF CFD CODES

Hugh M. McIlroy Jr., Donald M. McEligot,* and Robert J. Pink

Idaho National Laboratory
P.O. Box 1625
Idaho Falls, Idaho 83415

Abstract

The experimental program that is being conducted at the Matched Index-of-Refractive (MIR) Flow Facility at Idaho National Laboratory (INL) to obtain benchmark data on measurements of flow phenomena in a scaled model of the lower plenum of a typical prismatic gas-cooled reactor (GCR) using 3-D Particle Image Velocimetry (PIV) is presented. A detailed description of the model, scaling, the experimental facility, 3-D PIV system, measurement uncertainties, experimental procedures and samples of the data sets that have been obtained are included. Samples of the data set that are presented include mean-velocity-field and turbulence data in an approximately 1:7 scale model of a region of the lower plenum. This experiment has been selected as the first Standard Problem endorsed by the Generation IV International Forum.

Results concentrate on the region of the lower plenum near its far reflector wall (away from the outlet duct). Inlet jet Reynolds numbers (based on the jet diameter and the time-mean flow rate) are approximately 4,300 and 12,400. The measurements reveal undeveloped, non-uniform flow in the inlet jet ducts and complicated flow patterns in the modeled lower plenum. Data include three-dimensional vector plots, data displays along the coordinate planes (slices) and charts that describe the component flows at specific regions in the model. Information on inlet flow is also presented.

1. INTRODUCTION

The Very High Temperature Reactor (VHTR) is the most likely candidate for the Next Generation Nuclear Plant (NGNP). Because of the high temperatures characteristic of the VHTR, it is important to be able to simulate the turbulent flow in the reactor, especially in the lower plenum in order to ensure that large temperature gradients are not present in the coolant that could adversely impact structural materials. It is recognized that to simulate the flow in the VHTR lower plenum, advanced CFD codes using appropriate turbulence modeling will be necessary.

The objectives of the experimental and computational research programs conducted at INL are (1) to build accurate, reliable numerical simulation models of important VHTR thermal-hydraulic phenomena, (2) to provide benchmark data for the assessment and improvement of thermal-hydraulic codes proposed for evaluating the VHTR designs, and (3) to begin preliminary code development and assessment tasks based on identified modeling needs and existing data.

Feasibility studies for VHTR designs will require accurate, reliable predictions of material temperatures to evaluate the material capabilities. In a prismatic VHTR, these temperatures depend on the thermal convection in the coolant channels for the core and in other important components. Unfortunately, correlations in one-dimensional system codes for gas-cooled reactors typically underpredict these temperatures, particularly in reduced-power operations and hypothesized-accident scenarios. Likewise, some turbulence models in general purpose CFD codes provide optimistic predictions in the sense that surface temperatures are typically under-predicted (Mikielewicz et al., 2002 and Richards et al., 2004). These treatments are further complicated by the non-homogeneous power

* Professor Emeritus, University of Arizona, and presently on sabbatical leave at IKE, University of Stuttgart

distributions with strong peaking that can occur, in addition to buoyancy, strong pressure gradients and gas property variations in the channels. The U.S. Department of Energy (DOE) needs improved modeling capabilities, independent from the sometimes simplistic approaches employed by reactor vendors. These computational capabilities need, in turn, to be validated by comparison to experimental and analytical benchmark data.

McEligot et al. (2005) reported six areas of thermal hydraulic phenomena in which the application of improved CFD and system thermal-hydraulic analytical techniques can be used in the design and safety analyses of a prismatic VHTR. Several of these phenomena are pertinent to pebble bed versions of the VHTR as well. Initial studies concentrate on coolant flow distribution through the reactor core channels and mixing of hot jets in the reactor lower plenum. These phenomena are important both in normal operation and in accident scenarios. This paper addresses the mixing of hot jets in the lower plenum of the reactor.

INL has developed a large Matched-Index-of-Refractive (MIR) flow system that uses optical techniques, such as laser Doppler velocimetry (LDV) and PIV, to obtain flow field measurements in complex passages without disturbing the flow. The refractive indices of the fluid and the model are matched so that there is no optical distortion. The large size provides good spatial and temporal resolution and provides a means to measure flow fields, turbulence and mixing in the complex geometry of a prismatic VHTR lower plenum. The resulting data may be employed to assess CFD codes and their turbulence models for the limiting case of dominant forced convection where temperature can be considered to be a passive scalar. A code must be validated against these data before it can be considered for extension to include more complicated phenomena (e.g., buoyancy influences, property variation).

The general approach of the overall project is to develop new benchmark experiments for assessment in parallel with CFD and coupled CFD systems code calculations for the same geometry (see Johnson et al. (2006)). The velocity and turbulence fields measured in the MIR flow system will be used to assess the capabilities of the CFD codes and their turbulence models and to provide guidance in improving the models. A model of the lower plenum based on the point design of the NGNP (MacDonald et al., 2003) was developed and employed in this experiment.

McEligot and McCreery (2004) conducted scaling studies and conceptual designs for flow and heat-transfer experiments intended to assess CFD codes and their turbulence models proposed for application to prismatic VHTR concepts. Condie et al. (2005) documented the design of the present experiment to measure generic flow phenomena expected to occur in the lower plenum of a typical prismatic VHTR. The products of these efforts resulted in the fabrication and installation of a scaled model of the region of a typical VHTR lower plenum that is near the outer reflector wall, away from the plenum outlet.

The objective of this paper is to document the data set that has been established as benchmark data for flow phenomena in a lower plenum model of a typical prismatic gas-cooled reactor for the validation (as defined by Roach (1988)) of CFD codes.

2. MODEL SCALING

Prismatic NGNP concepts were examined to identify their proposed geometries and flow conditions at nominal full-power operation and at ten per cent power. Approximate analyses were applied to determine key non-dimensional parameters and their magnitudes at these two power levels.

2.1 Scaling Model Inlet Flow from the Reactor Core Cooling Channels

In the prismatic NGNP Point Design the cooling channels are simple vertical, circular tubes with complexity arising due to the spatial variations in local fission rate and the temperature dependencies of the gas properties. Scaling studies, conceptual experiment designs for application to the lower plenum experiment and estimates of some of the non-dimensional parameters are presented in McEligot and McCreery (2004). The scaling studies and estimates based on the coolant channel designs for the standard

fuel blocks and the control blocks indicate that quasi-fully-developed, turbulent flow is expected in the cooling channels.

Also, the Reynolds number based on gas bulk velocity and hydraulic (or jet) diameter, Re , non-dimensional heat flux, q^+ , acceleration parameter, K_r (for streamwise acceleration as density decreases), and a buoyancy parameter, Bo^* were estimated at the entrance, mid-height and exit of the coolant channels (for both power levels) (see McEligot and McCreery (2004) for a discussion of these non-dimensional parameters). These estimates establish that the range of duct outlet Reynolds numbers varied from about 57000 for the nominal full-power level to about 2300 at the ten per cent power level. Additionally, over this range q^+ , K_r and Bo^* were sufficiently low relative to their thresholds to establish that the flow from the outlets of the jet inlet ducts would be turbulent and that acceleration, buoyancy effects and gas property variation across the channels would not be significant.

2.2 Scaling Model Lower Plenum Flow

As shown in Figures 1 and 2, the hot flow from the coolant channels through the lower plenum to the hot core outlet duct encounters a very complicated geometry. Flow from the coolant channels is brought to the corners of the lower reflector blocks supporting the active core (see Figure 1). At these corners short ducts carry the flow vertically down into short inlet ducts above the plenum. From the inlet ducts the flow emerges into the plenum as hot jets. The cross sections and flow rates of these ducts differ depending on whether the corners -- at which they are located -- are common to three, two or one active column. There are four rows of jets under the active core then none under the central reflector, as in the model (see Figure 2). In the plenum, circular graphite posts support the active core and the inner and outer reflector columns; differing diameters of these posts lead to differing pitch-to-diameter ratios in the array of posts.

The flow in the lower plenum can locally be considered to be multiple jets streaming into a confined density-stratified crossflow with obstructions. Since the flow converges ultimately to a single lower plenum outlet, the hot jets encounter different crossflow velocities depending on their locations relative to the outlet. The jets furthest from the plenum outlet essentially exhaust into stagnant surroundings between the posts near the reflector wall and the reflector wall, with the exception of the flow which the jets induce. The last row of jets before the plenum outlet encounters cross-flow from all the other jets.

For a single-hole corner channel (i.e., the duct along the corner of a single active outer column with two inactive solid columns adjacent), the bulk velocity at 1000 °C is about 25 m/s (80 ft/s) and the resulting jet Reynolds number is about 90,000. One might expect these jets to travel along the corners of the adjacent solid vertical reflector-wall as wall jets and then to impinge on the plenum floor. A plenum Reynolds number at the passage between the first row of posts encountered would be about 24,000, based on the hydraulic diameter of the opening between the posts.

For the flow between the row of posts before the last row of jets near the plenum outlet, the plenum bulk velocity would be about 40 m/s (130 ft/s), still a low Mach number. The plenum Reynolds number in this region would be about 3×10^6 . The velocity ratio V_J/V_P would be about 0.6. Even without buoyancy effects (if the jet is hot relative to the crossflow) and drag by nearby posts, the estimated jet penetration would be less than two jet diameters which would be less than a fifth of the

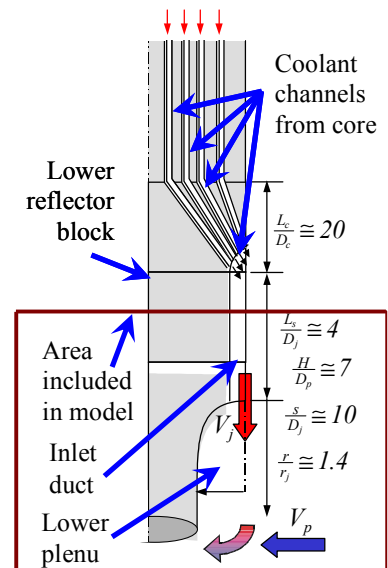


Fig. 1: Diagram of transition from coolant channels to jet inlet to lower plenum in typical NGNP concept.

distance to the plenum floor. Estimation of the acceleration parameter, for flow from the lower plenum converging into the plenum outlet duct, indicated that laminarization might occur at reduced power but not in normal full power operations. Approximate analyses were conducted to examine whether significant influences of buoyancy should be expected for the jets entering the lower plenum or for the near horizontal flow within it. Nominal operating conditions were considered. For a 300 °C temperature difference and $T_b = 1000$ °C, the approximations indicate that the jets should be considered to be effectively momentum-driven at full power and at one-tenth power. That is, buoyancy in the jets would not be expected to have a significant influence on jet interactions with the flow in the plenum.

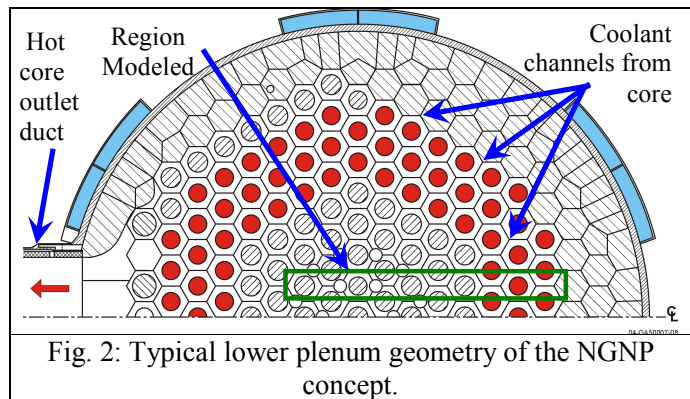
A second approximate analysis was conducted to estimate when a temperature gradient will stabilize a horizontal turbulent channel flow, thereby leading to reduced thermal transport near the upper surface. The analysis concluded that for full power, buoyancy influences are probably not important, but for ten per cent power, buoyancy may be important at the side of the lower plenum away from the plenum outlet but not near the plenum outlet.

Thus, experiments without buoyancy effects (as in those conducted in the INL Matched-Index-of-Refractive Flow System) should provide useful benchmark data for assessing CFD codes for some lower plenum flows.

3. Matched-Index-of-Refractive Facility

Velocity field measurements were taken in the MIR closed-loop flow system located at INL in Idaho Falls, Idaho (Figure 3). Stoots et al. (2001) presents a detailed review of this system. The system consists of a stainless steel closed flow loop with three polycarbonate and glass test sections. The facility can operate with water or light mineral oil as working fluid. The working fluid for this experiment was light mineral oil that is circulated (clockwise in Figure 3) by an axial pump powered by a 56 kW (75-hp) variable speed electric motor that can provide a maximum volumetric flow rate of approximately 0.6 m³/s of mineral oil through the test section. This maximum volumetric flow rate corresponds to a maximum test section inlet velocity of approximately 1.7 m/s. The test section includes three chambers that are constructed of 3.8 cm thick polycarbonate supported by a stainless steel framework. Each chamber is fitted with a removable lid. The test section inside dimension is 0.61m square and it is 2.44 m long. Both sides of each chamber of the test section are equipped with glass window inserts in the side panels to accommodate high quality measurements with LDV and/or PIV systems..

Mineral oil in the primary flow loop flows around the model for temperature control of the external surfaces of the model. The mineral oil temperature is maintained with a temperature control loop as shown in the lower right corner of Figure 3. The temperature control loop extracts approximately 300 L/min of mineral oil from the primary flow loop and pumps it through a glycol-cooled heat exchanger and a 10 kW DC heater where it is filtered, and then re-injected into the primary flow loop. This temperature control system can maintain the fluid temperature in the test section to within ± 0.05 °C of the specified index-matching temperature. An additional auxiliary flow loop (shown in the upper left corner of Figure 3), with a similar temperature control system, is used to provide fluid for the interior-model flows. Fluid is extracted from the primary flow loop and routed to a 5 kW (7 hp) pump that produces flow to the model inlet jets. To maintain the required working fluid temperature, a portion of this fluid is extracted from the auxiliary flow loop and routed through a parallel auxiliary temperature control loop. As in the primary temperature control loop, the mineral oil is cooled and reheated before returning to the



auxiliary flow loop and into the model inlet jets. Control instrumentation includes thermistors, flow meters, data acquisition, and computer controls.

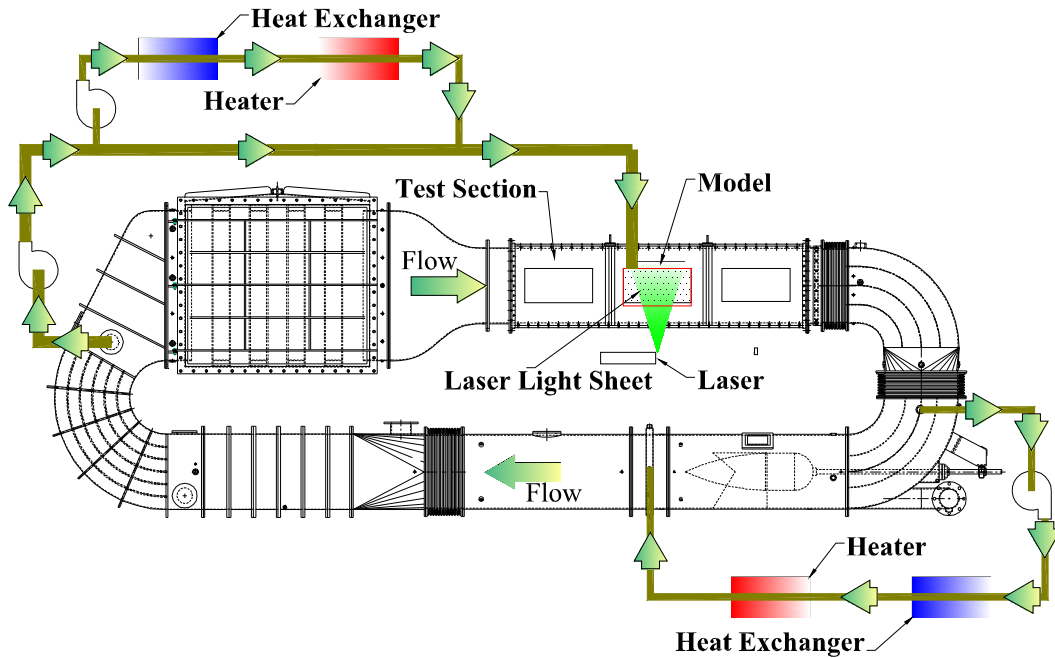


Fig. 3: MIR Facility.

4. PARTICLE IMAGE VELOCIMETRY (PIV) SYSTEM

Velocity field measurements were obtained with a 3-D PIV system from LaVision, Inc^{*}. The 3-D PIV system consists of two ImagerPro Plus digital CCD cameras and a double-pulsed Nd: YAG laser from Big Sky Laser. The system is controlled with DaVis 7.1 software. DaVis is a CCD image acquisition program developed by LaVision and controlled by a LaVision dual-processor Programmable Timing Unit (PTU). The PIV system cameras are mounted on a 3-directional traverse system that is controlled by three separate electric stepping motors. The cameras can be positioned and re-positioned to within 2 μm accuracy using linear stages and digital readouts at the operator's station. The spanwise laser position is also controlled with an electric stepping motor. The laser can be positioned to within 5 μm with an optical linear stage on the laser and a digital readout located at the operator's station. The PIV system laser was mounted below the test section (Figure 3) and produced a vertical light sheet approximately 2 mm thick. Both of the PIV system cameras were mounted on one side of the test section and aligned in a horizontal plane for camera views effectively normal to the vertical light sheet.

4.1 Seeding Particle Effects on Mineral Oil Flow

^{*} References herein to any specific commercial product, process, or service by trade name, trademark, manufacturer, or otherwise, does not necessarily constitute or imply its endorsement, recommendation, or favoring by the U.S. Government, any agency thereof, or any company affiliated with the Idaho National Laboratory.

One approach to examine the question of particle motion, relative to fluid motion i.e., to what extent the measured particle velocities represent the desired fluid velocities, is in terms of settling velocity or terminal velocity due to gravity. The terminal velocity for a small particle falling through a stagnant fluid due to gravitational forces can be estimated via a force balance for steady motion,

$$\frac{dV}{dt} = 0 = \left(\frac{4}{3}\right)\pi a^3 (\rho_p - \rho_f) - 6\pi \mu_f a \phi V \quad (1)$$

where a is the particle diameter, ρ_p is the particle density, ρ_f is the fluid density, μ_f is the fluid viscosity, and V is the settling velocity. The first term is the difference between the gravitational force and buoyancy while the second represents drag on the particle. The quantity, ϕ is a correction factor relative to Stokes drag; it approaches unity as the particle Reynolds number approaches zero. This relation can be rearranged to yield the settling velocity as

$$V \approx \left(\frac{2a^2 g}{9\nu\phi}\right) \left[\left(\frac{\rho_p}{\rho_f}\right) - 1\right]. \quad (2)$$

For our particles of about 1.7 g/cc and radii of 10 μm , this estimate gives about 0.02 mm/s or less and $\text{Re}_p \approx 3 \times 10^{-5}$. The lowest flow velocity we might encounter is about 1 cm/s. Thus, from this approach the particles are expected to follow the flow adequately.

A second approach is to examine the particle drift velocity and density effects as described by Foster (2005). Foster described the particle drift velocity as

$$V \approx \frac{(\rho_p - \rho_f)}{18 \cdot \mu_f} \cdot d_p^2 \cdot g \quad (3)$$

where d_p is the particle diameter. Additionally, Foster reports that a density ratio greater than ~ 0.1 would indicate that turbulent effects are significant. For this second approach, our particle drift velocity is approximately 7.5×10^{-7} m/s and the density ratio is approximately 7.9×10^{-6} . Therefore, since both values are negligible both particle drift and turbulence effects are expected to be insignificant.

5. EXPERIMENTAL MODEL

Figure 4 is a photograph of the model that was installed in the MIR test section. The model is fabricated from fused quartz and carefully positioned, located and fixed in the test section (see Appendix A by Condie et al. (2005) for detailed drawings of the model). Table 1 lists some of the key parameters of the model. Mineral oil from the auxiliary loop enters into the model jets on the top of the model via two inlet jet elbow manifolds like the aluminum manifold shown on top in Figure 4. The four inlet jet flow rates are individually controlled and measured by large Series 2600 Hi-Accuracy Flowmeters from Flowmetrics, Inc. The four inlet jet flows merge in the lower plenum and flow toward the outlet (left) end of the model where the flow exits and merges with the primary loop flow. The four jet inlet flows are individually conditioned in the elbow manifolds to model flow characteristics expected to be present in the actual GCR cooling channels that the inlet jets are simulating. Key requirements for the inlet-jet flows are that they are moderately turbulent, uniform and contain negligible swirl. When the working fluids

reach the inlet jet elbow manifolds the flows are turned and straightened, then pass through a honeycomb, through a screen, and finally through a turbulence generator to induce desired levels of turbulence before entering the inlet jets.

6. EXPERIMENTAL PROCEDURES

The primary loop axial flow pump circulated the mineral oil around the exterior of the model for index-matching temperature control (see Table 2). A jet Reynolds number of 4300 was chosen because it

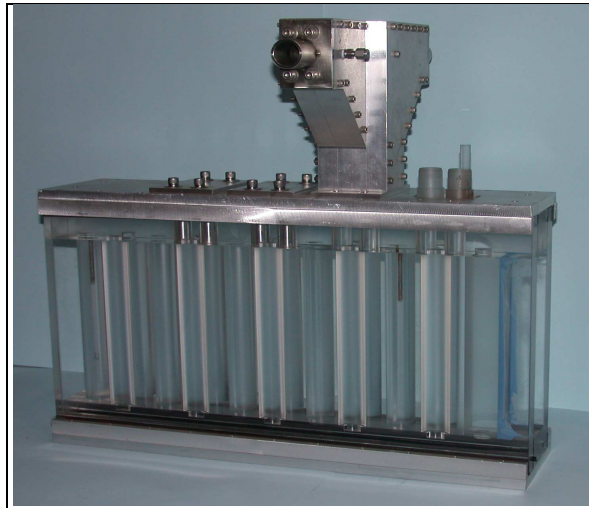


Fig. 4: Quartz model.

Table 1: Model Parameters	
<i>Properties</i>	<i>Value</i>
Model length	558.80 mm
Model height	306.40 mm
Model width	104.78 mm
Channel height	217.50 mm
Channel width	53.98 mm
Post height	217.5 mm
Jet inlet diameter	22.10 mm
Centerline distance between posts	93.50 mm
Ratio of plenum height to post diameter	6.85
Ratio of jet diameter to post diameter	0.7
Ratio of channel width to post diameter	1.7
Post diameter	31.75 mm

was the lowest Reynolds number that would reasonably produce a mixed-turbulent flow in the lower plenum. The higher Reynolds number (12400) was the largest Reynolds number attainable in our system.

The temperatures of both the primary flow loop and auxiliary flow loop were controlled with LabVIEW™ software. The temperature control system maintained the oil temperature to within ± 0.05 °C of the calculated index-matching temperature (~ 23.3 °C) in the model and to within ± 0.03 °C of the index matching temperature in the primary flow loop. The facility remained at a constant, steady state condition throughout the data collection periods. Temperature records for all data collection files are archived on the temperature control computer. Laser power, Q-Switch delays, and the time between frames of the double-image cameras (dt) were adjusted using the Interactive Mode in the DaVis 3-D PIV software.

Table 2: MIR Facility and PIV Parameters		
<i>Parameter</i>	<i>Re_J 4300</i>	<i>Re_J 12400</i>
MIR		
Main lop flow (m/s)	0.18	0.23
Jet No. 1 Flow Rate (gpm)	11.25	32.11
Jet No. 2 Flow Rate (gpm)	16.75	48.14
Jet No. 3 Flow Rate (gpm)	16.75	48.14
Jet No. 4 Flow Rate (gpm)	16.75	48.14
PIV		
Pixel size	7.4 μm	7.4 μm
Interrogation window	64x64-50% overlap then 32x32-50% overlap	64x64-50% overlap then 32x32-50% overlap
Camera Mode	3-D Cross Correlation	3-D Cross Correlation
Image Acquisition Method	RAM (fast)	Standard
Acquisition – Number of Images	170	750

In an effort to balance the requirement for high resolution data and to keep the size of data files within reasonable limits (for data processing and data storage considerations), the collection effort on the model was divided into eight regions. The lower plenum area of the model was divided into six regions and, for

the higher Re_j flow study, the inlet jet area was divided into two regions (one region for each pair of jets). Additionally, in order to collect (3-D) data across the entire width of the model channel (spanwise) the laser and cameras were sequentially positioned at 23 different spanwise planes. The laser-light sheet was adjusted to a thickness of about 2 mm which allowed for complete coverage of the model except for an area near the model walls where the laser-light sheet was blocked by O-ring seals. Therefore, each region of the lower plenum consisted of 23 PIV image files—one file for each spanwise plane. The inlet-jet regions only required 11 planes/files to cover the full width of the jets.

Because of the refractive index difference between the air space where the cameras operated and the mineral oil where the light sheet was located, it was necessary to coordinate the movement of the two digital cameras relative to the movement of the laser-light sheet. This coordination was accomplished with a MATHCAD code. The code used the mineral oil temperature to determine the index of refraction of the mineral oil and the camera angles relative to the laser-light sheet reported by the camera calibration procedure to calculate a movement ratio for the camera movement relative to the laser light sheet movement. This ratio was typically between 0.62 and 0.68, that is, for a movement ratio of 0.66, a 2 mm shift of the laser-light sheet required the camera support to be moved about 1.32 mm. Table 2 summarizes the settings used on the MIR facility and PIV systems.

Data post-processing of the acquired images was accomplished with DaVis 7.1 software. The post-processed data were then transferred from DaVis to a secondary PC where data were organized and displayed with TecPlot 360™ and/or MS Excel software. The total processing time exceeded 900 hours of computer time and produced approximately 2 TB of data.

7. UNCERTAINTY ESTIMATES

The objective of uncertainty analysis is to develop an understanding of the estimated experimental uncertainties in the results. For proper benchmark databases, the experimental uncertainties of all measured quantities and their propagation into the results must be obtained quantitatively. In a complicated experiment such as this, some experimental uncertainties can be expected to vary significantly with position as the local velocities vary. McEligot et al. (2007) present a detailed analysis of the experimental uncertainty estimates for this study. Table 3 is a list of some of the uncertainty estimates.

8. EXPERIMENTAL RESULTS

The objective of the experimental program was to obtain velocity field measurements for CFD code assessment. To accomplish this objective the flow inside the lower plenum model was characterized with velocity-vector fields and fourteen scalar quantities. McIlroy et al. (2007) provide a list that defines the vector and scalar field measurements that were obtained. Since uniform time intervals were employed, the time-mean statistics are calculated from suitable arithmetic averages of the stored data.

The data set presented here is a sample of the high flow ($Re_j \sim 12400$) data available for code assessment. Due to the tremendous volume of data obtained and the complicated nature of the flow, only

<i>Parameter</i>	<i>Uncertainty</i>	<i>Parameter</i>	<i>Uncertainty</i>
Pixel displacement	0.3 pixels	Image distance	± 0.16 mm
Timing	$\sim 0.001\%$	Fluid temperature	± 0.05 °C
Lightsheet thickness	10%	Fluid density	$\sim 0.2\%$
Velocity	$\sim 0.3\%$ - 1.2%	Dynamic viscosity	$\sim 2\%$
Turbulence intensity	$\sim 1.8\%$	Kinematic viscosity	$\sim 0.2\%$
Scatter in velocity statistics	$\sim 0.4\%$ - 10%	Refractive index	$\sim 0.02\%$
Mean square fluctuations	$\sim 1.3\%$ - 6%	Geometry	$\sim 0.2\%$
Camera position	± 2 μ m	Flow rates	0.8% - 8.4%
Laser position	± 5 μ m	Reynolds numbers	1%

a brief analysis is presented. Data at specific locations will be presented along with a brief description of some of the major phenomena observed in the flow.

Figure 5 is a mean vector plot of the flow along the centerline of the model calculated from 750 PIV image pairs. The white regions between the vector groups represent the model support posts. Flow enters the model vertically from the four inlet jets located at the top-right corner of the plot and streams downward into the lower plenum where it interacts with the support posts and reflector wall, and then gradually turns toward the left and flows toward the model exit located to the left of the figure. The dashed line in the diagram above the figure shows the location of this data plane. Figure 6 is a streamline plot of this flow.

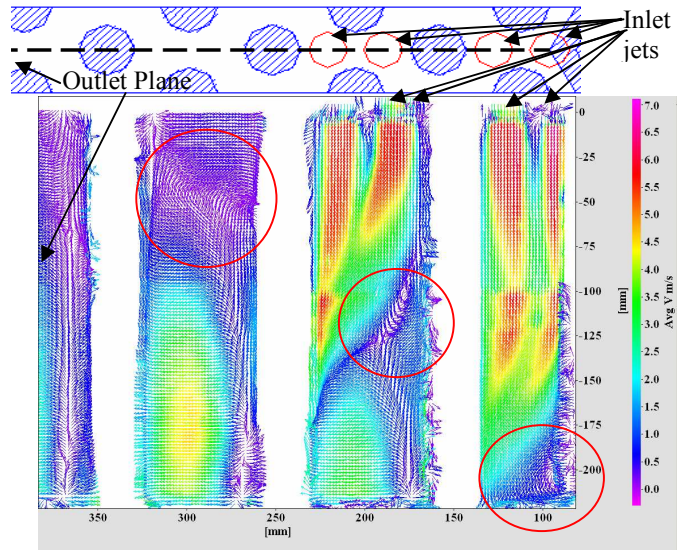


Fig. 5: Mean Vector Field for $Re_j \sim 12400$.

Three major structures are visible in Figures 5 and 6 as shown by the three red circles: the recirculation zone in the lower right corner, the recirculation zone near the mid-height of the model between the first two support posts, and the recirculation zone near the top of the model on the downstream side of the second and third support posts. Three secondary structures are also visible: the line of merging flow below the two downstream (left) pair of jets and just downstream of the first support post from the bottom of the model to just below the second recirculation zone noted above, the line of merging flow just downstream of the second support post, and the line of merging flow that extends along the full model height on the downstream side of the third support post.

The first recirculation zone is formed by the first pair of inlet jets and their interaction with the reflector wall, first support post, and the bottom of the model. The flows from the two jets merge quickly near the top of the model and are channeled downward between the first support post and reflector wall. As the flow approaches the bottom of the plenum the major portion of this flow turns to the left, flows around the first support post, and interacts with the flow from the second pair of jets. A small portion of this flow is forced to the right where it encounters the reflector wall and creates a recirculation zone. Some of this recirculating fluid is forced up the reflector wall where it interacts with the downward flow from the jets and is subsequently reversed and forced toward the bottom of model plenum.

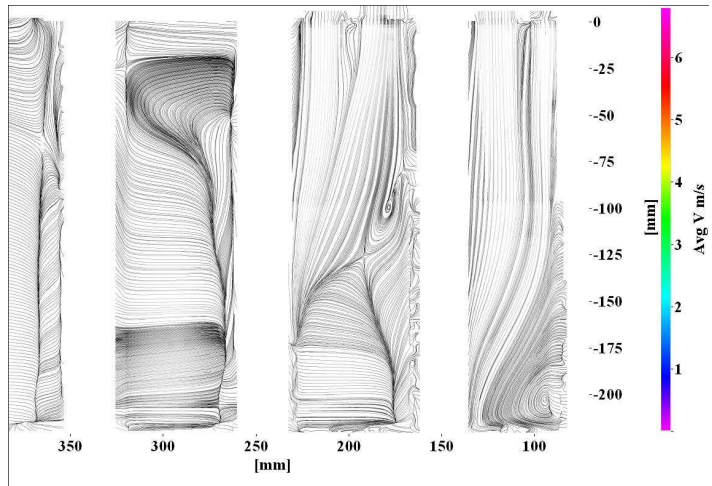


Fig. 6: Mean Streamlines for $Re_j \sim 12400$.

The second major structure is the recirculation zone that is formed by the flow from the second pair of jets. These flows also merge near the top of the plenum and are channeled downward in the area between the first and second support posts where they interact with the flow from the first (upstream) pair of jets that has passed around the first support post. This interaction results in a portion of the flow rising up the downstream edge of the first support post,

causing a second recirculation zone about half way up the downstream edge of the first support post. The remainder of the flow generates a wake behind the lower portion of the second support post and then begins to flow toward the model exit (toward the left).

The third major structure is formed as the flows from both jet pairs merge and begin to flow toward the exit and interact with the second support post. Because no fluid is entering the plenum downstream of the second support post (no inlet jets above this region which corresponds to the central section of an annular core/plenum), the fluid flows around the second post, forms a wake and begins to rise to fill the upper portion of the model.

A portion of this flow near the top of the plenum is moves to the right on the downstream side of the second support post, and then downward forming the third recirculation zone. The flows in the bottom half of the model on the downstream side of the second support post merge and move toward the model exit. The flow then moves around the third support post, merges in a wake on the downstream side of the post, and gradually flows toward the left and slightly upward as it moves toward the model exit.

Finally, a small recirculation zone is evident on the downstream side of the third support post. This flow appears to be a result of the recirculating flow on the upstream side of the post. On the downstream side of the post the upper portion of the flow moves downward until it joins the flow moving upward from the bottom of the model. These two flows merge and move around the post where they join the recirculation zone between the second and third posts.

Figure 7 displays values of mean V_y (vertical velocity component) on a plane along the centerline of the model in the regions below the four inlet jets. The small diagram above the figure describes the spanwise location of the data slice. At the $y \sim -70$ mm below the top of the plenum, the vertical velocity under the jets (vertical momentum with no imposed crossflow) is substantial and downward. Lower in the plenum (at $y \sim -150$ mm), the flow under the

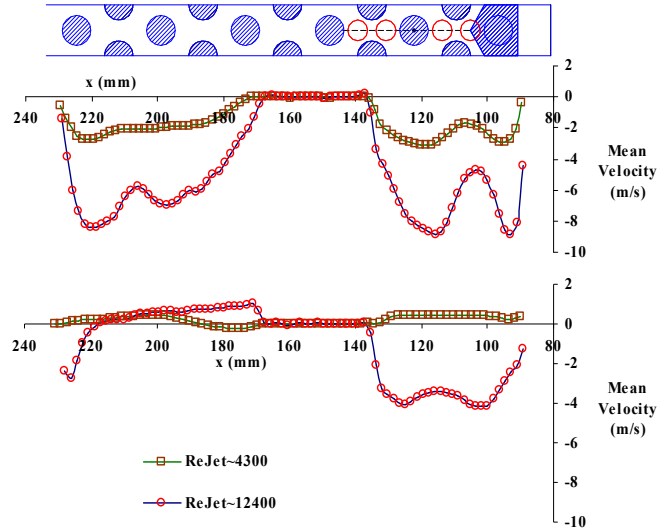


Fig. 7: Mean V_y along model centerline beneath four inlet jets at $y \sim -70$ mm (top) and $y \sim -150$ mm (bottom).

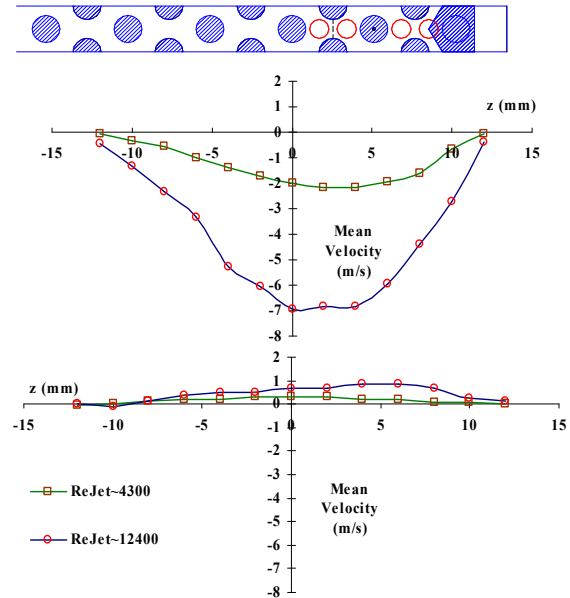


Fig. 8: Mean V_y along spanwise plane between jets 3 and 4 at $y \sim -70$ mm (top) and $y \sim -150$ mm (bottom).

jets in the Re_j 4300 case has reversed (flows slightly upward) and the flow in the Re_j 12400 case shows a flow reversal (slightly upward flow) under jets 3 and 4.

Figure 8 displays values of mean V_y (vertical velocity component) in a spanwise line from the vertical data slice between the posts below jets 3 and 4 as shown in the diagram above the figure. At $y \sim 70$ mm depth, the vertical velocity is substantial and negative (downward) from the inlet-jet flows entering the lower plenum from jets 3 and 4. Lower in the plenum (at $y \sim 150$), the vertical flow reverses and moves upward to form the lower part of the recirculation zone noted earlier. The asymmetry in the flow in Figure 8 is due to asymmetries in the inlet jet flows caused by the model of the outer reflector wall and differences in the flows (see Figure 9).

Figure 9 displays the inlet jet mean V_y (vertical) velocity profiles within the jet inlet ducts for the Re_j 12400 case. The dashed lines represent the centerline location of the inlet duct walls. Jet No. 1 is on the right, inlet jets 2, 3, and 4 are to the left. The profiles were measured at a level inside the inlet ducts 11 mm above the opening into the plenum ($y/D_j \sim 0.5$ to the exit plane).

The eleven velocity profiles near the exit of each jet inlet duct display developing, turbulent flow in the ducts. Jet No. 1 is smaller than the other jets because 1/3 of this jet is filled, as in a prismatic reactor, by the reflector wall. These profiles were extracted from the raw data files using the locations of the jets from fabrication drawings and analysis of the flows close to the jet walls. It is noteworthy that results of numerical integrations using both the Trapezoid Rule and Simpson's Rule produce an inlet volume flow rate of 169.7 gpm – which is only 3.9% less than the volume flow rate measured by calibrated flow meters upstream of the jets. The estimated uncertainty in the measured flow rate is approximately 1% - 3% and the estimated uncertainty in the integrated flow rate is approximately 0.4% to 1.2%.

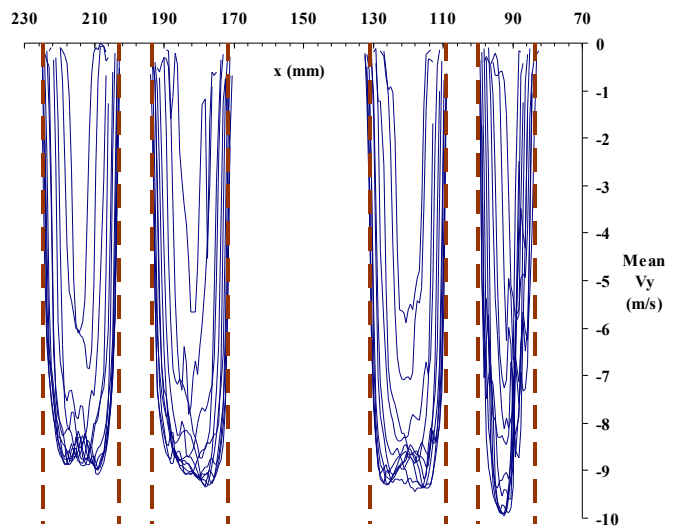


Fig. 9: Mean V_y in inlet jets for $Re_j \sim 12400$ at $y \sim 11$ mm ($y/D_j \sim 0.5$), -10 mm $< z < +10$ mm ($0 < r/r_j < 0.9$) @ 2 mm intervals.

9. STANDARD PROBLEM

A challenge of designing and licensing the VHTR is to confirm that the intended analysis tools can be used confidently to make decisions and to assure that the reactor systems are safe and meet the performance objectives of the Generation IV Program. The research and development projects at INL will ensure that the tools used to perform the required calculations and analyses are accurate and reliable.

CFD analyses will be a major component in the analysis suite that will be required to design and license the VHTR so the reactor can operate at maximum outlet temperatures and efficiencies. Only CFD analysis tools have the capability to determine where localized hot spots will occur in the reactor and also whether or not unacceptably large thermal gradients are present.

The calculational envelope of the CFD tools used to analyze the behavior of the VHTR is defined by the scenarios and phenomena that these tools can calculate with confidence. CFD tools can only be used confidently when the results they produce have been shown to be in reasonable agreement with first-principle results, thought-problems, and data that describe the “highly ranked” phenomena inherent in all operational conditions and important accident scenarios for the VHTR. Reasonable agreement is achieved

when the calculation generally lies within the uncertainty band of the data used for validation and always shows the same trends as the data and when code deficiencies are minor.

Presently, the CFD tools to be used for analyzing the VHTR are not ready to perform design and analysis, nor are they ready for licensing calculations to the standard that will be required by the VHTR. Considerable validation and, perhaps, development of the software tools is required. Additionally, practices and procedures are required for both validating and developing the necessary CFD software that are acceptable to the nuclear community.

The validation process is based on developing a set of standard problems that will populate a validation matrix for the various tools. The standard problems are defined by the Generation IV International Forum Standard Problem Committee, which defines its standard problems on the basis of comprehensive phenomena identification and ranking tables (PIRT) (Lee et al., 2005). The standard problems, which are defined using high-quality data sets with known uncertainty bands, are the measures used to determine whether or not an analysis tool is capable of calculating the required phenomena. The members of the Standard Problem Committee are experts in the potential scenarios that are projected to be important in the VHTR.

The standard problems are passed to the Problem Oversight Committee. Members of this committee are experts in using and validating the analysis tools. Some members of this committee were specifically chosen due to their expertise in other industries where CFD is widely used. This committee defines the practices and procedures that must be used to perform the standard problems, and they also distribute the standard problem to the participants. Finally, the Problem Oversight Committee is responsible for coordinating the comparisons between the participants' solutions and the experimental results, including the evaluation of the validation. It is understood that many of the standard problem's calculations will be "blind", that is, the participants will not be privy to the experimental data while their calculation is in progress.

Standard problems form the basis for determining whether a software tool is capable of analyzing the behavior of a reactor system undergoing a review for an operating license. The term "standard problem" stems from the use of the data sets that make up these problems as a measure (hence, a standard) to determine the acceptability of the software.

Standard problems consist of data sets that have the following characteristics:

a. The data set describes a phenomenon, or a set of phenomena, that influences the behavior of an important figure-of-merit. That is, given that the figure-of-merit is the reactor vessel wall temperature, which must be less than a predetermined value, then important phenomena are those that significantly influence the reactor vessel wall temperature. Such phenomena are identified in phenomena identification and ranking studies and are documented (Lee et al., 2005). An example of such a phenomenon is the turbulent mixing of hot exit gases in the lower plenum of the reactor vessel because hot jets with an above-average temperature may impinge on the outlet plenum wall and perhaps cause a local hot spot on the reactor-vessel wall.

b. The phenomenon given in the standard problem data set, although it may be measured in a reduced-scale system, can be scaled to the full-sized system using accepted scaling practices. The scaling studies that link the experimental apparatus and data to the full-sized system are documented in a report.

c. The standard problem data set has been shown to measure the data required to determine whether the software systems are capable of calculating the important phenomenon.

d. The standard problem data set has uncertainties associated with each data point.

e. The quality assurance procedures used to design the experiment, build the experiment, and conduct the experiment are consistent with NQA-1 requirements.

The experiment and results summarized in this paper are intended to assess CFD software and the experiment described herein meets the requirements identified in subparagraphs a – e above.

10. CONCLUDING REMARKS

The model design and MIR flow facility produced satisfactory flow conditions, as recommended by

previous scaling studies and model design. As a result of the experiments described in this paper, the objective of developing benchmark databases for the assessment of CFD solutions of the momentum equations, scalar mixing and turbulence models for typical prismatic VHTR plenum geometries in the limiting case of negligible buoyancy and constant fluid properties has been met. Additionally, the data obtained from these experiments meet the requirements of a standard problem as defined above.

Preliminary measurements of velocity components have been compiled for a low-power case of $Re_J \sim 4300$, and detailed measurements of the flow field for the maximum achievable flow rate in the present MIR facility of $Re_J \sim 12400$ have also been completed. The data have been documented to identify and report estimated uncertainties of the measurements and have been collected into various formats suitable for release to the CFD community and others, as necessary. Future plans include distribution of instructions to obtain data sets and points of contact at INL.

11. ACKNOWLEDGMENTS

This manuscript has been authored by a contractor of the U.S. Government under DOE Contract DE-AC07-05ID14517. Accordingly, the U.S. Government retains a nonexclusive, royalty-free license to publish or reproduce the published form of this contribution, or allow others to do so, for U.S. Government purposes.

The authors also acknowledge the highly professional and timely support and assistance of Dr. Steven L. Anderson of LaVision, Inc., Professor Barton L. Smith of Utah State University, and Richard R. Schultz of INL for their assistance in this project.

12. NOMENCLATURE

Symbol	Definition	Symbol	Definition
D_C	Coolant channel diameter	r_J	Jet duct radius
D_J	Jet diameter	Re_{Jet}	Reynolds number based on jet diameter and jet bulk velocity
D_P	Support post diameter	T_b	Bulk temperature
gpm	Gallons per minute	V_J	Jet bulk velocity
H	Lower plenum height	V_P	Plenum bulk velocity
L_C	Coolant channel length	x	Streamwise (model length) direction
L_S	Support block length	y	Vertical (model height) direction
r	Radius	z	Spanwise (model thickness) direction

13. REFERENCES

- K.G. Condie, G.E. McCreery, H.M. McIlroy Jr. and D.M. McEligot, "Development of an Experiment for Measuring Flow Phenomena Occurring in a Lower Plenum for VHTR CFD Assessment," *INL External Report INL/EXT-05-00603*, (September 2005).
- R.E. Foster, "Wave Behavior and Film Turbulence Measurements in Two Phase Flow," Master of Science Thesis, Univ. of Wisconsin-Madison, (2005).
- R.W. Johnson, D.P. Guillen and T. Gallaway, "Investigations of the Application of CFD to Flow Expected in the Lower Plenum of the Prismatic VHTR," *INL/EXT-06-11756*, (September 2006)
- W.J. Lee, K.D. Kim, M.K. Hwang, H.S. Lim, S.W. Lee, T.Y.C. Wei, R.B. Vilim, E.E. Feldman, W.D.R. Pointer, R.R. Schultz, P.D. Bayless and R.L. Moore, "Generation of a Preliminary PIRT (Phenomena Identification and Ranking Table) for Very High Temperature Gas-Cooled Reactors," *KAERI/TR-3050/2005*, *INL/EXT-05-00829*, or ANL-GenIV-066, (September 2005).
- P.E. MacDonald, J.W. Sterbentz, R.L. Sant, P.D. Bayless, R.R. Schultz, H.D. Gougar, R.I. Moore, A.M.

- Ougouag and W.K. Terry, "NGNP Preliminary Point Design – Results of the Initial Neutronics and Thermal-Hydraulic Assessments," *INEEL Technical Report INEEL/EXT-03-00870, Rev. 1*, (September 2003).
- D.M. McEligot and G.E. McCreery, "Scaling Studies and Conceptual Experiment Designs for NGNP CFD Assessment," *INL External Report INEEL/EXT-04-02502*, (November 2004).
- D.M. McEligot, K.G. Condie, G.E. McCreery, H.M. McIlroy Jr., R.J. Pink, L.E. Hochreiter, J.D. Jackson, R.H. Pletcher, B.L. Smith, P. Vukoslavcevic, J.M. Wallace, J.Y. Yoo, J.S. Lee, S.T. Ro and S.O. Park, "Advanced Computational Thermal Physics (CTFP) and its Assessment for Light Water Reactors and Supercritical Reactors," *INEEL Technical Report INL/EXT-05-00901*, (October 2005).
- D.M. McEligot, H.M. McIlroy Jr. and R.C. Johnson, "Estimated Uncertainties in the Idaho National Laboratory Matched-Index-of-Refractive Lower Plenum Experiment," *INL External Report INL/EXT-07-13539*, pp. 8-14 (November, 2007).
- H.M. McIlroy Jr., D.M. McEligot and R.J. Pink, "Measurement of Turbulent Flow Phenomena for the Lower Plenum of a Prismatic Gas-Cooled Reactor," *Proceedings, 12th International Meeting on Nuclear Reactor Thermal Hydraulics*, September 30 – October 4, Pittsburgh, PA, Log No. 67, (2007).
- D.P. Mikielewicz, A.M. Shehata, J.D. Jackson and D.M. McEligot, "Temperature, Velocity and Mean Turbulence Structure in Strongly-Heated Internal Gas Flows Comparison of Numerical Predictions with Data," *Int. J. Heat Mass Transfer*, Vol. 45, 4333-4352, (2002).
- A.H. Richards, R.E. Spall, and D.M. McEligot, "An Assessment of Turbulence Models for Strongly Heated Internal Gas Flows," *Proceedings of the Fifteenth IASTED International Conference on Modeling and Simulation Conference*, Marina Del Ray, CA., 1-3 March, 119-124, (2004).
- P.J. Roach, *Verification and Validation in Computational Science and Engineering*, Hermosa, Albuquerque, NM, USA, p 271, 1998.
- C. Stoots, S. Becker, K. Condie, F. Durst, and D.M. McEligot, "A Large-Scale Matched Index of Refraction Flow Facility for LDA Studies Around Complex Geometries," *Exp. in Fluids*, Vol. 30, pp. 391-394, (2001).